Topological transitions in dissipatively coupled Su-Schrieffer-Heeger models

Jayakrishnan M. P. Nair [1,2,*] Marlan O. Scully [1,2,3,4,†] and Girish S. Agarwal [1,2,‡]

[1] *Institute for Quantum Science and Engineering, Texas A&M University, College Station, Texas 77843, USA*

[2] *Department of Physics and Astronomy, Texas A&M University, College Station, Texas 77843, USA*

[3] *Baylor University, Waco, Texas 76704, USA*

[4] *Princeton University, Princeton, New Jersey 08544, USA*

(Received 11 September 2023; revised 6 November 2023; accepted 8 November 2023; published 21 November 2023)

Non-Hermitian topological phenomena have gained much interest among physicists in recent years. In this paper, we expound on the physics of dissipatively coupled Su-Schrieffer-Heeger (SSH) lattices, specifically in systems with bosonic and electrical constituents. In the context of electrical circuits, we demonstrate that a series of resistively coupled LCR circuits mimics the topology of a dissipatively coupled SSH model. In addition, we propose a scheme to construct dissipatively coupled SSH lattices involving a set of noninteracting bosonic oscillators weakly coupled to engineered reservoirs of modes possessing substantially small lifetimes when compared to other system timescales. Further, by activating the coherent coupling between bosonic oscillators, we elucidate the emergence of nonreciprocal dissipative coupling, which can be controlled by the phase of the coherent interaction strength precipitating in phase-dependent topological transitions and skin effect. Our analyses are generic, apropos of a large class of systems involving, for instance, optical and microwave settings, while the circuit implementation represents the most straightforward of them.

DOI: 10.1103/PhysRevB.108.184304

I. INTRODUCTION

One of the prime objectives of research in condensed matter physics is the characterization of matter phases earmarked by the (spontaneous breaking of) symmetries of the system under consideration. In this context, the discovery of the quantum Hall effect marked a stark shift in the understanding of phases by introducing the concept of topological order and thereby spawning the field of topological insulators [1–3]. This was subsequently realized on a variety of different platforms, including photonic [4], cold atomic systems [5], and many more [6–8]. One of the key features of the topological classification of phases is the bulk boundary correspondence (BBC) and the emergence of edge and surface states that are impervious to environmental loss and disorder with applications ranging from the realization of topological qubits [9–13] to lasing [14–17] among others [18–25].

Until recently, the lion's share of research on the physics of topological systems involved Hermitian models. However, real physical systems interact with their environment resulting in open quantum dynamics [26] and effective non-Hermitian Hamiltonians. In the last few years, the topology of non-Hermitian lattice systems has been a subject of intense research activity [27,28], unraveling some exciting new physics, for example, the breakdown of BBC and skin effect [29–39]. A quintessential model in the study of topological physics is the Su-Schrieffer-Heeger (SSH) model [40–44] and several non-Hermitian extensions of the model have been considered in literature [45–49]. For instance, [47,48,50] considered PT-symmetric extensions of the SSH model, which can be engineered by the incorporation gain into the system. While lattice models with gain and loss have been studied in Refs. [51–53], we note that non-Hermiticity can also be introduced via introducing asymmetric left and right hopping rates [31,32,34,54,55]. However, the physics of lattice models with a purely dissipative form of coupling [56,57] between the constituents is largely unplumbed. Dissipative coupling between two otherwise noninteracting systems emanates from their decay into common dissipative channels [58]. In an early work [26] it was shown quite generally that many systems interacting with a common bath exhibit both dissipative and dispersive couplings [59]. In another study [60], a more general form of dissipative coupling was derived for a system interacting with a bath possessing phase-sensitive correlations [61]. It is worth noting that dissipative couplings are more prevalent in nature compared to their coherent counterparts. Such couplings have been investigated both theoretically and experimentally in a multitude of settings [59,61–66], for example, involving magnonic and photonic subsystems [67–71].

In this work, we focus on the physics of dissipatively coupled SSH models. In particular, we demonstrate two distinct experimentally realizable schemes involving bosonic and electrical subsystems. We show that a system of resistively coupled LCR resonators mimics the topology of dissipatively coupled SSH (DSSH) models. Subsequently, we illustrate that a lattice of otherwise noninteracting bosonic oscillators interacting with engineered reservoirs of modes having significantly large decay parameters compared to other system parameters can be described by an effective non-Hermitian Hamiltonian akin to the DSSH model. Furthermore, by

*Present address: Department of Physics, Boston College, 140 Commonwealth Avenue, Chestnut Hill, Massachusetts 02467, USA; muttathi@bc.edu

†scully@tamu.edu

‡Girish.Agarwal@ag.tamu.edu

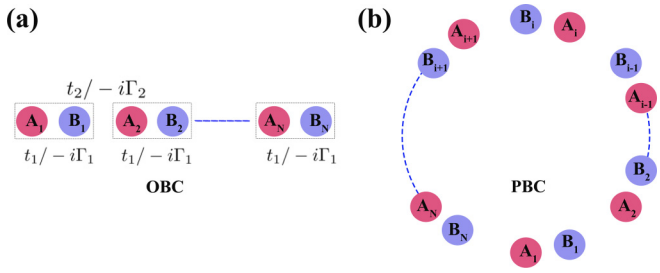

FIG. 1. Schematic of the system described by Eqs. (1)–(2) and Eq. (7) under open and periodic boundary conditions.

triggering the coherent coupling between the oscillators, we outline the generation of nonreciprocal coupling in DSSH models featuring topological transitions that can be controlled by the phase of the coherent interaction strength. Note, *en passant*, the generality of our results grant an immediate experimental realization of the protocols discussed in the subsequent sections, especially in the microwave and optical domains.

This paper is organized as follows. In Sec. II, we revisit the SSH model with coherent couplings followed by a discussion of its dissipative counterpart in Sec. III. Subsequently, we delineate two independent schemes comprised of electrical and bosonic constituents for the realization of the DSSH model in Sec. IV. In Sec. V, we feature a protocol for the realization of DSSH model with nonreciprocal couplings through the application of a coherent form interaction between bosonic oscillators, translating into topological transitions and skin effect. Finally, we conclude our results in Sec. VI.

II. KEY FEATURES OF THE SSH MODEL

We begin by revisiting the SSH model coherently coupled unit cells. To this end, consider a one-dimensional (1D) lattice of two different types of sites, A and B with staggered nearest-neighbor couplings as depicted in Fig. 1. The interaction Hamiltonian of the system subject to open boundary conditions (OBC) is given by

$$H = \sum_{i=1}^{N} t_1 |A_i\rangle\langle B_i| + \sum_{i=1}^{N-1} t_2 |A_{i+1}\rangle\langle B_i| + \text{H.c.}, \tag{1}$$

where N denotes the number of unit cells, $|A_i\rangle$, $|B_i\rangle$ characterize the particle excitation at their respective location while t_1 and $t_2 \in \mathbb{R}$ are the intra- and intercellular couplings, respectively. Equivalently, we can write the SSH Hamiltonian subject to periodic boundary conditions (PBC) as

$$H = \sum_{i=1}^{N} t_1 |A_i\rangle\langle B_i| + \sum_{i=1}^{N} t_2 |A_{f(i)}\rangle\langle B_i| + \text{H.c.}, \tag{2}$$

where $f(i) = i + 1 \bmod N$. Invoking the Bloch theorem, the Hamiltonian under PBC can be recast in the Fourier domain in terms of the Bloch Hamiltonian provided by

$$H_k = \begin{pmatrix} 0 & R(k)e^{-i\phi(k)} \\ R(k)e^{i\phi(k)} & 0 \end{pmatrix}, \tag{3}$$

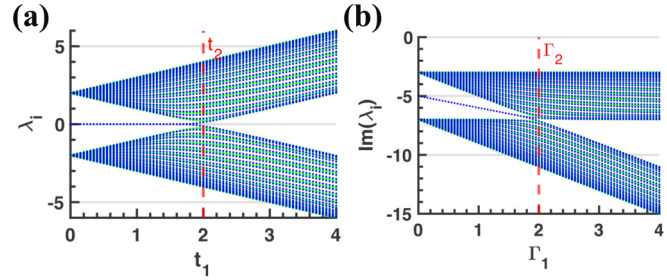

FIG. 2. (a) The eigenvalues of the Hermitian SSH model described by Eqs. (1)–(2) under periodic (green) and open (blue) boundary conditions. (b) The imaginary part of the eigenvalues of the dissipative SSH model described by Eq. (7) under periodic (green) and open (blue) boundary conditions and the number of unit cells $N = 25$ and the effective damping $\Gamma_R = \gamma + \Gamma_1 + \Gamma_2$ and $\gamma = 3$.

where $k = \frac{2\pi n}{N}$, $m \in \{1, 2, \ldots, N\}$, $R(k) = \sqrt{t_1^2 + t_2^2 + 2t_1 t_2 \cos(k)}$, the phase $\phi(k) = \arctan(\frac{t_2 \sin k}{t_1 + t_2 \cos k})$ and we set the intercellular spacing $a = 1$. Note that the Hermitian matrix H_k is chiral symmetric, that is $\sigma_z H_k \sigma_z = -H_k$ precipitating in symmetric eigenvalues $E_\pm = \pm R(k)$ and corresponding eigenstates

$$|E_\pm, k\rangle = \frac{1}{\sqrt{2}} \begin{pmatrix} \pm 1 \\ e^{i\phi(k)} \end{pmatrix}. \tag{4}$$

Palpably, the gap between the energy eigenvalues vanishes at $k = \pi$ and $t_1 = t_2$ as demonstrated in Fig. 2(a). In contrast, the Hamiltonian under OBC described by Eq. (1) supports two zero-energy eigenvalues in the large N limit for $|\frac{t_1}{t_2}| < 1$, eliciting the well-known edge modes of the SSH model, a testament to the nontrivial topology of the system. In addition, one can define a topological invariant, *viz*, the winding number $\nu_\pm$ defined in terms of the Berry connection $A_\pm(k) = i\langle E_\pm, k|\partial_k|E_\pm, k\rangle$ as

$$\nu_\pm = \frac{1}{\pi} \oint A_\pm(k) dk. \tag{5}$$

For instance, ν_+ calculated from Eq. (4) and Eq. (5) satisfies

$$\nu_+ = \begin{cases} 1 & \text{if } \left|\frac{t_1}{t_2}\right| < 1 \\ 0 & \text{if } \left|\frac{t_1}{t_2}\right| > 1 \end{cases}. \tag{6}$$

A nonzero winding number $\nu_\pm$ is a direct manifestation of the nontrivial topology of the system demonstrating $2|\nu_\pm|$ number of edge modes and $t_1 = t_2$, the point of vanishing gap between bulk energy bands demarcates the boundary between the two phases. This is known as the bulk boundary correspondence (BBC) in Hermitian lattice systems. It is worth noting that coherent coupling between systems emanates from the spatial overlap between their respective modes. By contrast, dissipatively coupled systems with a non-Hermitian form of interaction are prevalent in nature. In essence, any two systems interacting with a common intermediary channel will spawn a dissipative form coupling. In the following, we will discuss the general properties of dissipatively coupled SSH models.

III. DISSIPATIVELY COUPLED SSH (DSSH) MODEL

Consider a 1D lattice of sites A and B coupled dissipatively as depicted in Fig. 1. This is analogous to the Hermitian SSH model, except for a notable difference in the off-diagonal elements, wherein, the real couplings t_1 and t_2 are now replaced by purely imaginary numbers leading to an effective non-Hermitian Hamiltonian given by

$$\begin{aligned} H = &-\sum_{i=1}^{N}((\Delta_1 - i\Gamma_R)|A_i\rangle\langle A_i| + (\Delta_2 - i\Gamma_R)|B_i\rangle\langle B_i|) \\ &+ \sum_{i=1}^{N} i\Gamma_1|A_i\rangle\langle B_i| + \sum_{i=1}^{N-1} i\Gamma_2|A_{i+1}\rangle\langle B_i| \\ &+ \sum_{i=1}^{N} i\Gamma_1|B_i\rangle\langle A_i| + \sum_{i=1}^{N-1} i\Gamma_2|B_i\rangle\langle A_{i+1}|, \end{aligned} \tag{7}$$

where $\Gamma_R = \gamma + \Gamma_1 + \Gamma_2$ denotes the effective damping constant corresponding to A_i and B_i and we assume modes A_i and B_i decay at the same rate γ. The emergence of an effective Hamiltonian describing the above equation from considerations of a real-space Hermitian system will be explicated in subsequent sections. For simplicity, we set $\Delta_1 = \Delta_2 = 0$. The effective Bloch Hamiltonian under PBC is provided by

$$\mathcal{H}(k) = \begin{pmatrix} -i\Gamma_R & i\Gamma_1 + i\Gamma_2 e^{-ik} \\ i\Gamma_1 + i\Gamma_2 e^{ik} & -i\Gamma_R \end{pmatrix}, \tag{8}$$

with eigenvalues $E_\pm = -i\Gamma_R \pm i\sqrt{\Gamma_1^2 + \Gamma_2^2 + 2\Gamma_1\Gamma_2\cos k}$ where $k = \frac{2\pi n}{N}$, the parameters Γ_j, $j \in \{1, 2\}$ are the absolute value of the strength of dissipative coupling and we have set the diagonal elements to be identical. Owing to the non-Hermitian nature of the system, the right eigenvectors and their dual left eigenvector basis of $\mathcal{H}(k)$ are, in general, not identical. Let $|R_\pm, k\rangle$ and $|L_\pm, k\rangle$ be the biorthogonal right and left eigenvectors, respectively, of $\mathcal{H}(k)$ defined by

$$\begin{aligned} \mathcal{H}(k)|R_\pm, k\rangle &= E_\pm|R_\pm, k\rangle \\ \mathcal{H}^\dagger(k)|L_\pm, k\rangle &= E_\pm^*|L_\pm, k\rangle, \end{aligned} \tag{9}$$

such that $\langle L_m, k|R_n, k\rangle = \delta_{m,n}$ where $m, n \in \{+, -\}$ and $\delta_{m,n}$ is the Kronecker delta. Interestingly, $\mathcal{H}(k)$ is anti-Hermitian, i.e., $\mathcal{H}^\dagger(k) = -\mathcal{H}(k)$. As a result, the biorthogonal eigenvectors have the property

$$|R_\pm, k\rangle = |L_\pm, k\rangle = \frac{1}{\sqrt{2}}\begin{pmatrix} 1 \\ \pm ie^{i\phi(k)} \end{pmatrix}, \tag{10}$$

where $\phi(k) = -\arctan(\frac{\Gamma_1 + \Gamma_2\cos k}{\Gamma_2 \sin k})$. Subsequently, one can define the Berry connection involving the biorthogonal eigenvectors as $A_\pm(k) = i\langle L_\pm, k|\partial_k|R_\pm, k\rangle$ and analogous to the Eq. (5) of coherently coupled SSH model, the system is topological with $\nu_+ = 1$ for $|\Gamma_2| > |\Gamma_1|$. Note, *en passant*, the constant diagonal decay is irrelevant for topological considerations. An interesting consequence of non-Hermiticity is the breakdown of BBC. In other words, the parameters corresponding to the energy gap closing in a non-Hermitian Bloch Hamiltonian do not, in general, signify the boundary between topological and trivial phases. On the contrary, owing to the anti-Hermitian nature of $\mathcal{H}(k)$, the dissipatively coupled system described in Fig. 1 follows BBC. In Fig. 2(b), we plot the eigenvalues of the system under PBC and OBC and when $|\frac{\Gamma_1}{\Gamma_2}| < 1$, it displays the conspicuous emergence of two distinct eigenvalues corresponding to the edge modes flanked on either side by the bulk modes. Not surprisingly, this is exactly the point of the vanishing energy gap between the Bloch modes corroborating BBC.

Role of real diagonal terms in DSSH. Consider now the scenario $\Delta_1 = -\Delta_2 = \Delta$. The Bloch Hamiltonian under PBC modifies to

$$\mathcal{H}_k = \begin{pmatrix} \Delta - i\Gamma_R & h(k) \\ -h^*(k) & -\Delta - i\Gamma_R \end{pmatrix}, \tag{11}$$

where $h(k) = i\Gamma_1 + i\Gamma_2 e^{-ik}$. Observe that the effective momentum space Hamiltonian is anti-PT symmetric, in other words, $(\hat{PT})\mathcal{H}_k(\hat{PT}) = -\mathcal{H}_k$. We may rewrite $h(k) = B_x - iB_y$, where $B_x = \Gamma_2\sin(k)$ and $B_y = -[\Gamma_1 + \Gamma_2\cos(k)]$ are pseudomagnetic fields providing an analogy to spin-half particles interacting with magnetic fields. When discussing the topological properties of the system, the constant diagonal term $-i\Gamma_R$ is irrelevant. The eigenvalues of the system, ignoring $-i\Gamma_R$ are given by $E_\pm = \pm\sqrt{\bar{\Delta}^2 - (B_x^2 + B_y^2)}$ for $|\bar{\Delta}| > |h(k)|$ and $E_\pm = \pm i\sqrt{B_x^2 + B_y^2 - \bar{\Delta}^2}$ for $|\bar{\Delta}| < |h(k)|$. Here, we focus on the region where $|\bar{\Delta}| < |h(k)|$ and use the parametrization $\frac{\bar{\Delta}}{R} = \sinh(\theta)$, $\frac{B_x}{R} = \cosh(\theta)\cos(\phi)$, $\frac{B_y}{R} = \cosh(\theta)\sin(\phi)$, where $R = \sqrt{B_x^2 + B_y^2 - \bar{\Delta}^2}$ to obtain the right and left eigenvectors of the eigenvalue λ_+ as

$$|R_+\rangle = \frac{1}{\sqrt{2[1 + i\sinh(\theta)]}}\begin{pmatrix} -i\cosh(\theta)e^{-i\phi} \\ 1 + i\sinh(\theta) \end{pmatrix} \tag{12}$$

$$|L_+\rangle = \frac{1}{\sqrt{2[1 + i\sinh(\theta)]}}\begin{pmatrix} -i\cosh(\theta)e^{-i\phi} \\ 1 - i\sinh(\theta) \end{pmatrix}. \tag{13}$$

The Berry connection of the system is defined as $A_+(k) = i\langle L_+|\partial_k|R_+\rangle$. Utilizing the parametrization discussed above, we can recast the Berry connection as $A(k) = (\partial_k\phi)A(\phi) + (\partial_k\theta)A(\theta)$. If we consider, for example, a trajectory in the θ-ϕ space, wherein, $\partial_k\theta = 0$, the Berry connection is given by $A(k) = \frac{1}{2}(1 - i\sinh(\theta)\partial_k\phi$. Note, when $\theta = 0$, the equation for winding number

$$\nu_+ = \frac{1}{\pi}\oint A_+(k)dk, \tag{14}$$

morphs into Eq. (5) and the system is topological with $\nu_+ = 1$ for $|\Gamma_2| > |\Gamma_1|$. More precisely, the anti-PT-symmetric system demonstrates partial topological phases for trajectories where $\partial_k\theta = 0$, wherein, the real part of the winding numbers mimics the topology of a Hermitian SSH model. It is worth noting that the Hamiltonian $\mathcal{H}_k$ is not chiral symmetric, in other words $\sigma_z\mathcal{H}_k\sigma_z \neq -\mathcal{H}_k$. In the following section, we provide two experimentally realizable protocols to engineer DSSH model.

IV. REALIZATION OF THE DISSIPATIVE SSH MODEL

Circuit model. In this section, we provide a circuit model to construct the DSSH model employing an electrical circuit involving coupled amplifying LRC resonators connected in parallel through a coupling resistor as depicted in Fig. 3. Upon

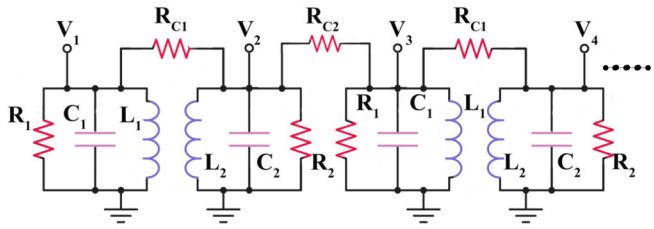

FIG. 3. Circuit model consisting of resistively coupled LCR resonators for the realization of dissipatively coupled SSH model resulting in the dynamics described by Eq. (15).

solving for Kirchhoff's equations of motion for voltages, we obtain

$$\ddot{V}_n + \omega_1^2 V_n + (\gamma_1 + \Gamma_1 + \Gamma_2)V_n = \Gamma_1 \dot{\bar{V}}_n + \Gamma_2 \dot{\bar{V}}_{n-1}$$
$$\ddot{\bar{V}}_n + \omega_2^2 \bar{V}_n + (\gamma_2 + \Gamma_1 + \Gamma_2)\bar{V}_n = \Gamma_1 \dot{V}_n + \Gamma_2 \dot{V}_{n+1}. \quad (15)$$

Here, $\omega_1 = 1/\sqrt{L_1 C_1}$, $\omega_2 = 1/\sqrt{L_2 C_2}$, $\Gamma_1 = \frac{1}{R_{c1} C_1}$, $\Gamma_2 = \frac{1}{R_{c2} C_2}$, $\gamma_i = \frac{1}{R_i C_i}$, and $L_{1,2}, R_c, C_{1,2}$ are, respectively, inductance, the two coupling resistances, capacitance of the constituent elements in the unit cell and we assume $C_1 = C_2$. Note, *en passant*, the constants Γ_1 and Γ_2 represent the intra- and intercellular couplings in the lattice. In the weak coupling and small detunings regime, that is, when $\{\Gamma_1, \Gamma_2\} \ll \{\omega_1, \omega_2\}$ and $|\omega_1 - \omega_2| \ll \frac{\omega_1+\omega_2}{2}$, we can reduce the above equations by using the slowly varying envelope functions $v_n(t)$, $\bar{v}_n(t)$, such that

$$V_n(t) = \frac{v_n(t)e^{-i\omega_0(t)} + \text{c.c.}}{2}$$
$$\bar{V}_n(t) = \frac{\bar{v}_n(t)e^{-i\omega_0(t)} + \text{c.c.}}{2}, \quad (16)$$

where $\omega_0 = \frac{\omega_1+\omega_2}{2}$. Employing Eq. (16), the dynamics of the envelope functions are obtained as

$$\dot{v}_n = -i\frac{\bar{\Delta} - i(\gamma_1 + \Gamma_1 + \Gamma_2)}{2} v_n + \frac{\Gamma_1}{2}\bar{v}_n + \frac{\Gamma_2}{2}\bar{v}_{n-1}$$
$$\dot{\bar{v}}_n = i\frac{\bar{\Delta} + i(\gamma_2 + \Gamma_1 + \Gamma_2)}{2} \bar{v}_n + \frac{\Gamma_1}{2} v_n + \frac{\Gamma_2}{2} v_{n+1}, \quad (17)$$

with $\bar{\Delta} = \frac{\omega_1-\omega_2}{2}$. We assume propagating solutions for the sublattice elements, that is,

$$v_n = \sum_k v_{k,\omega} e^{i(kn-\omega t)} + \text{c.c.}$$
$$\bar{v}_n = \sum_k \bar{v}_{k,\omega} e^{i(kn-\omega t)} + \text{c.c.}, \quad (18)$$

where k is the wave vector and the lattice constant is taken to be unit. Substituting Eq. (18) into Eq. (17), we arrive at the eigenvalue equation $(H_k - \omega)X = 0$, where $X^T = [\, v_{k,\omega} \;\; \bar{v}_{k,\omega}]$ and

$$H_k = \begin{pmatrix} \bar{\Delta} - i(\gamma_1 + \Gamma_1 + \Gamma_2) & i\left(\frac{\Gamma_1}{2} + \frac{\Gamma_2}{2}e^{-ik}\right) \\ i\left(\frac{\Gamma_1}{2} + \frac{\Gamma_2}{2}e^{-ik}\right) & -\bar{\Delta} - i(\gamma_2 + \Gamma_1 + \Gamma_2) \end{pmatrix}. \quad (19)$$

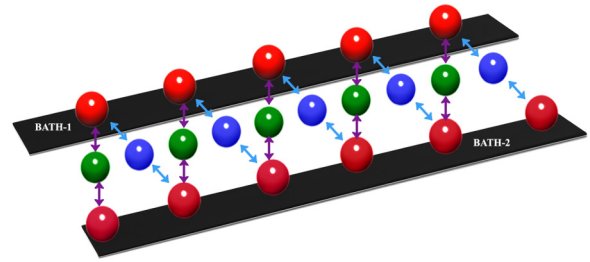

FIG. 4. Schematic of the coupled oscillator system described by the Hamiltonian in Eq. (20) comprising of a bath of oscillators coupled with a system of otherwise noninteracting bosonic modes. The red spheres of bath-1 (bath-2) denote the modes a_i (d_i) beginning on the left from a_1 (d_0). The green (blue) spheres represent the modes b_i (c_i) beginning on the left from b_1 (c_1).

The Hamiltonian H_k is equivalent to $\mathcal{H}_k$. In other words, the circuit lattice is topologically equivalent to a dissipatively coupled SSH model.

Photonic systems. We begin by considering the following generic Hamiltonian comprising of a chain of coherently coupled bosonic sublattice elements a_i, b_i, c_i, and d_i under OBC as depicted in Fig. 4.

$$\mathcal{H}/\hbar = \sum_{i=1}^{N} \omega_{b,i} b_i^\dagger b_i + \sum_{i=1}^{N} \omega_{c,i} c_i^\dagger c_i + \sum_{i=1}^{N} \omega_{a,i} a_i^\dagger a_i$$
$$+ \sum_{i=0}^{N} \omega_{d,i} d_i^\dagger d_i + \sum_{i=1}^{N} [g_1 b_i^\dagger (a_i + d_{i-1}) + h.c]$$
$$+ \sum_{i=1}^{N} [g_2 c_i^\dagger (a_i + d_i) + \text{H.c.}] \quad (20)$$

Here, $\omega_{x,i}$ characterizes the resonance frequencies of the modes x_i, where $x \in \{a, b, c, d\}$ and g_1, $g_2 \in \mathbb{R}$ are the strength of dispersive coupling between the modes. We assume that all the modes b_i and c_i decay at approximately the same rate γ whereas the modes a_i and d_i decay at rates κ_1 and κ_2, respectively. Further, we set $\Delta_{b,i} = \Delta_1 = \omega_{b,1} - \omega_{a,1}$, $\Delta_{c,i} = \Delta_2 = \omega_{c,1} - \omega_{a,1}$, $\omega_{a,i} = \omega_{d,i} = \omega_{a,1}$, and $\kappa_1 > \kappa_2$. In the weak coupling domain, that is, when the leakage rates κ_i strongly dominates the dynamics of the system, in other words, $\{g_1, g_2, \gamma, \Delta_{b,1}, \Delta_{c,1}\} \ll \{\kappa_1, \kappa_2\}$, we can adiabatically eliminate the a_i and d_i modes resulting in the effective momentum space Hamiltonian of the system under PBC ($d_0 = d_N$) in the frame rotating at $(\Delta_1 + \Delta_2)/2$ as (Appendix B)

$$\mathcal{H}_k = \begin{pmatrix} \bar{\Delta} - i\Gamma_R & h(k) \\ -h^*(k) & -\bar{\Delta} - i\Gamma_R \end{pmatrix}, \quad (21)$$

where we set $g_1 = -g_2 = g$, $\bar{\Delta} = (\Delta_1 - \Delta_2)/2$, $\Gamma_R = \gamma + \Gamma_1 + \Gamma_2$, $h(k) = i\Gamma_1 + i\Gamma_2 e^{-ik}$, and k is the lattice constant equivalent to Eq. (11) and $\Gamma_i = \frac{g^2}{\kappa_i}$. Note that the pair of modes b_i and c_i form a unit cell with intra- and intercell couplings $i\frac{g^2}{\kappa_1}$ and $i\frac{g^2}{\kappa_2}$, respectively, equivalent to the system in Fig. 1 under dissipative settings with Γ_i replaced by $\frac{g^2}{\kappa_i}$.

V. NONRECIPROCITY, PHASE-DEPENDENT TOPOLOGICAL TRANSITIONS, AND SKIN EFFECT

In the previous section, we briefly mentioned the breakdown of BBC in non-Hermitian systems. In particular, nonreciprocal (chiral) coupling between sublattice elements under OBC culminates in the skin effect, which is the exponential localization of right and left eigenvectors at the lattice boundaries without any distinction between bulk and edge modes. In addition, the points in the parametric space corresponding to the closing of energy gap under PBC do not indicate the emergence of eigenmodes with eigenvalues $-i\Gamma_{\rm R}$ under OBC requiring a biorthogonal modification of the BBC. In the following, we discuss the construction of nonreciprocal [53] couplings in DSSH lattice leading to phase-dependent topological transitions and skin effect.

Consider now a one-dimensional lattice of bosonic modes b, c coupled with auxiliary modes a as depicted in Fig. 4 where we have now switched on the coherent coupling between b_i and c_i modes. The system is characterized by the Hamiltonian

$$\tilde{\mathcal{H}}/\hbar = \mathcal{H}/\hbar + \sum_{i=1}^{N}[Gb_i^\dagger c_i + \text{H.c.}], \tag{22}$$

where $\mathcal{H}$ is given by Eq. (20) and $G = |G|e^{i\alpha}$. Once again, in the weak coupling domain, that is, when $\{g_1, g_2, |G|, \gamma\}$ are significantly less than the cavity leakage κ_i and setting $\Delta_{b,i} = \Delta_1 = \omega_{b,1} - \omega_{a,1}$, $\Delta_{c,i} = \Delta_2 = \omega_{c,1} - \omega_{a,1}$, $\omega_{a,i} = \omega_{b,i} = \omega_{a,1}$, $\kappa_1 > \kappa_2$, and $g_1 = -g_2 = g$, we can obtain an effective system between modes b_i and c_i. The system under PBC translates into the following Bloch Hamiltonian in the frame rotating at $(\Delta_1 + \Delta_2)/2$:

$$\mathcal{H}_k = \begin{pmatrix} \bar{\Delta} - i\Gamma_{\rm R} & i\Gamma_- + i\Gamma_2 e^{-ik} \\ i\Gamma_+ + i\Gamma_2 e^{ik} & -\bar{\Delta} - i\Gamma_{\rm R} \end{pmatrix}, \tag{23}$$

where $\Gamma_\pm = \Gamma_1 \mp |G|\sin\alpha - i|G|\cos\alpha$, $\bar{\Delta} = (\Delta_1 - \Delta_2)/2$, and $\Gamma_{\rm R} = \gamma + \Gamma_1 + \Gamma_2$.

Note that the non-Hermitian system described by the aforementioned Hamiltonian does not follow BBC. To elucidate this in detail, let us begin by considering the system under OBC. Before expounding the analysis of the full system, it is worthwhile to explicate the properties of the system in the absence of c_N and to simplify the analysis, we set $\bar{\Delta} = 0$ for the remaining part of this section. When the lattice terminates in b_N, the $(2N-1)$-dimensional Hamiltonian of the system $H^b_{\rm broken}$ supports biorthogonal eigenstates with eigenvalue $-i\Gamma_{\rm R}$ of the form [32,72]

$$|R\rangle^b = N_{\rm R}^b \sum_{n=0}^{N-1}\left(-\frac{\Gamma_2}{\Gamma_+}\right)^{N-n} b_{n+1}^\dagger|0\rangle$$
$$|L\rangle^b = N_{\rm L}^b \sum_{n=0}^{N-1}\left(-\frac{\Gamma_2}{\Gamma_-^*}\right)^{N-n} b_{n+1}^\dagger|0\rangle, \tag{24}$$

where $N_{\rm R}, N_{\rm L}$ are normalization constants such that $\langle L|R\rangle = 1$ provided by $N_{\rm L}^{b*}N_{\rm R}^b = Z^{N+1}\frac{(Z^{-1}-1)}{1-Z^N}$, $Z = \frac{\Gamma_-\Gamma_+}{\Gamma_2^2}$, and

$$H^b_{\rm broken} = \begin{bmatrix} -i\Gamma_{\rm R} & i\Gamma_- & 0 & 0 & \dots & 0 \\ i\Gamma_+ & -i\Gamma_{\rm R} & i\Gamma_2 & 0 & \dots & 0 \\ 0 & i\Gamma_2 & -i\Gamma_{\rm R} & i\Gamma_- & \dots & 0 \\ 0 & 0 & i\Gamma_+ & -i\Gamma_{\rm R} & \dots & 0 \\ 0 & 0 & \dots & \dots & \dots & i\Gamma_2 \\ 0 & 0 & \dots & \dots & i\Gamma_2 & -i\Gamma_{\rm R} \end{bmatrix}_{2N-1}. \tag{25}$$

This is due to destructive interference at c_i sites and observe that $|R\rangle^b$ and $|L\rangle^b$ can be written as a column matrix, for instance,

$$|R\rangle^b = \begin{bmatrix} \left(-\frac{\Gamma_2}{\Gamma_+}\right)^N \\ 0 \\ \left(-\frac{\Gamma_2}{\Gamma_+}\right)^{N-1} \\ \vdots \\ 0 \\ -\frac{\Gamma_2}{\Gamma_+} \end{bmatrix}_{2N-1}, \tag{26}$$

and clearly $H^b_{\rm broken}|R\rangle^b = -i\Gamma_{\rm R}|R\rangle^b$. Notice that when $\alpha = \pi/2$, Eq. (24) morphs into

$$|R\rangle^b = N_{\rm R}^b \sum_{n=0}^{N-1}\left(-\frac{\Gamma_2}{\Gamma_1 + |G|}\right)^{N-n} b_{n+1}^\dagger|0\rangle$$
$$|L\rangle^b = N_{\rm L}^b \sum_{n=0}^{N-1}\left(-\frac{\Gamma_2}{\Gamma_1 - |G|}\right)^{N-n} b_{n+1}^\dagger|0\rangle, \tag{27}$$

which is, identical to the results for a coherently coupled SSH model with nonreciprocal intracell couplings. By the same token, one can construct eigenstates of complex energy $-i\Gamma_{\rm R}$ of the Hamiltonian $H^c_{\rm broken}$ of the lattice which is broken at the other end, i.e., when the lattice ends on either side with c_i sites as

$$|R\rangle^c = N_{\rm R}^c \sum_{n=1}^{N}\left(-\frac{\Gamma_2}{\Gamma_-}\right)^{N} c_n^\dagger|0\rangle$$
$$|L\rangle^c = N_{\rm L}^c \sum_{n=1}^{N}\left(-\frac{\Gamma_2}{\Gamma_+^*}\right)^{N} c_n^\dagger|0\rangle, \tag{28}$$

where $N_{\rm L}^{c*}N_{\rm R}^c = N_{\rm L}^{b*}N_{\rm R}^b = Z^{N+1}\frac{(Z^{-1}-1)}{1-Z^N}$.

In stark contrast to Hermitian systems where the absolute value square of the coefficient of the column matrix in Eq. (26) would represent the probability of finding the excitation at the nth unit cell, non-Hermitian systems necessitate a biorthogonally defined projection to the nth unit cell. Subsequently, one can define a biorthogonal projection operator P_n to the nth unit cell of the lattice as $P_n = |b,n\rangle\langle b,n| + |c,n\rangle\langle c,n|$ where $|b,n\rangle = b_n^\dagger|0\rangle$ and $|c,n\rangle = c_n^\dagger|0\rangle$. For example, projecting the states in Eq. (24) on to the nth unit cell provides

$$\langle L|^b P_n|R\rangle^b = \frac{Z^{n+1}(Z^{-1}-1)}{1-Z^N}. \tag{29}$$

It is therefore apparent that for $|Z| < 1$, the excitation is exponentially localized at the left edge ($n = 1$) whereas $|Z| > 1$ localizes the state at the right edge $n = N$. Similarly, when the lattice terminates with a c_i mode on either side (b_1 is absent), one can obtain analogous results with the excitation localized at the right (left) edge for $|Z| < 1 (|Z| > 1)$ due to mirror symmetry.

The results of the broken chain system can now be used to extract the physics of the full system in the thermodynamic limit (large N). Consider the Hamiltonian of the full system

$$H_{\text{full}} = \begin{bmatrix} -i\Gamma_R & i\Gamma_- & 0 & 0 & \dots & 0 & 0 \\ i\Gamma_+ & -i\Gamma_R & i\Gamma_2 & 0 & \dots & 0 & 0 \\ 0 & i\Gamma_2 & -i\Gamma_R & i\Gamma_- & \dots & 0 & 0 \\ 0 & 0 & i\Gamma_+ & -i\Gamma_R & \dots & 0 & 0 \\ 0 & 0 & \dots & \dots & \dots & i\Gamma_2 & 0 \\ 0 & 0 & \dots & \dots & i\Gamma_2 & -i\Gamma_R & i\Gamma_- \\ 0 & 0 & \dots & \dots & 0 & i\Gamma_+ & -i\Gamma_R \end{bmatrix}_{2N}, \tag{30}$$

and states

$$|\psi\rangle_R^{\pm} = \frac{1}{\sqrt{2}}\left\{\begin{bmatrix} |R\rangle^b \\ 0 \end{bmatrix} \pm \begin{bmatrix} 0 \\ |R\rangle^c \end{bmatrix}\right\}$$
$$|\psi\rangle_L^{\pm} = \frac{1}{\sqrt{2}}\left\{\begin{bmatrix} |L\rangle^b \\ 0 \end{bmatrix} \pm \begin{bmatrix} 0 \\ |L\rangle^c \end{bmatrix}\right\}. \tag{31}$$

Clearly, $\langle\psi|_L^{\pm}|\psi\rangle_R^{\pm} = 1$ and $\langle\psi|_L^{\mp}|\psi\rangle_R^{\pm} = 0$ and it is straightforward to obtain

$$H_{\text{full}}|\psi\rangle_R^{\pm} = \begin{bmatrix} \mp i\Gamma_2 N_R^c \\ 0 \\ \vdots \\ 0 \\ -i\Gamma_2 N_R^b \end{bmatrix}_{2N} - i\Gamma_R|\psi\rangle_R^{\pm}$$
$$H_{\text{full}}^{\dagger}|\psi\rangle_L^{\pm} = \begin{bmatrix} \pm i\Gamma_2 N_L^c \\ 0 \\ \vdots \\ 0 \\ i\Gamma_2 N_L^b \end{bmatrix}_{2N} + i\Gamma_R|\psi\rangle_L^{\pm}, \tag{32}$$

where we have defined $N_R^b = N_R^c = \left(\frac{Z^{N+1}(Z^{-1}-1)}{1-Z^N}\right)^{1/2}$ and $N_L^b = N_L^c = N_R^{b*}$. It is conspicuous from the above expression that $|\psi\rangle_{R,L}^{\pm}$ represent biorthogonal eigenstates of H_{full} with complex energy $-i\Gamma_R$ for large N for $N_R^b \to 0$, *viz*, if $|Z| < 1$ (and not for $|Z| \geqslant 1$) as the normalization factors in the first part of the right-hand side (RHS) of Eq. (32) approach zero. In other words, the states in Eq. (31) are the eigenstates of H_{full} with eigenvalue $-i\Gamma_R$ (Γ_R modes) for

$$\sqrt{(\Gamma_1^2 - |G|^2)^2 + 4|G|^2\Gamma_1^2\cos^2\alpha} < \Gamma_2^2. \tag{33}$$

It is worth noting that for $\alpha = \pi/2$, the condition for biorthogonal edge modes modifies to $\Gamma_1^2 - |G|^2 < \Gamma_2^2$. The Eq. (33) may be rewritten as $(\Gamma_1^2 - A_+)(\Gamma_1^2 - A_-) < 0$, where

$$A_{\pm} = -|G|^2\cos(2\alpha) \pm \sqrt{\Gamma_2^4 - |G|^4\sin^2(2\alpha)} \tag{34}$$

for real values of the RHS of Eq. (34). Therefore, the Γ_R modes of the system under OBC occur in the region where $\Gamma_1^2 < A_+$ and $\Gamma_1^2 > A_-$. It is worth noting that the system does not incur Γ_R modes for $\Gamma_2^4 - |G|^4\sin^2(2\alpha) < 0$. In Fig. 5, we plot the absolute value of eigenvalues of the full system under OBC and PBC for different values of α and $|G|$ for $\Gamma_2 = 2$ where we have defined $x_{\pm} = \sqrt{A_{\pm}}$ for non-negative values of $A_{\pm}$. In Figs. 5(a)–5(b), for $|G| = 1$, we observe that $A_+ > 0$ and $A_- < 0$ lending Γ_R modes for $|\Gamma_1| < x_+$ depicted by the two isolated blue lines. In stark contrast, for $|G| = 3$ and $\alpha = \pi/4$, $\Gamma_2^4 - |G|^4\sin^2(2\alpha) < 0$, leading to the conspicuous absence of Γ_R modes as depicted in Fig. 5(c). However, $\alpha = \pi/2$, $|G| = 3$ [Fig. 5(d)] renders $A_{\pm} > 0$, which affords Γ_R-modes on either in the region $x_- < \Gamma_1 < x_+$, demonstrating phase dependent nature of topological transitions. Note that the green curves in Fig. 5 correspond to the absolute value of energy under OBC. Clearly, the points where the blue curves approach $-i\Gamma_R$ do not match with that of the green curves as a consequence of the breakdown of BBC. In Fig. 6, we plot the phase (not to be confused with α) diagram

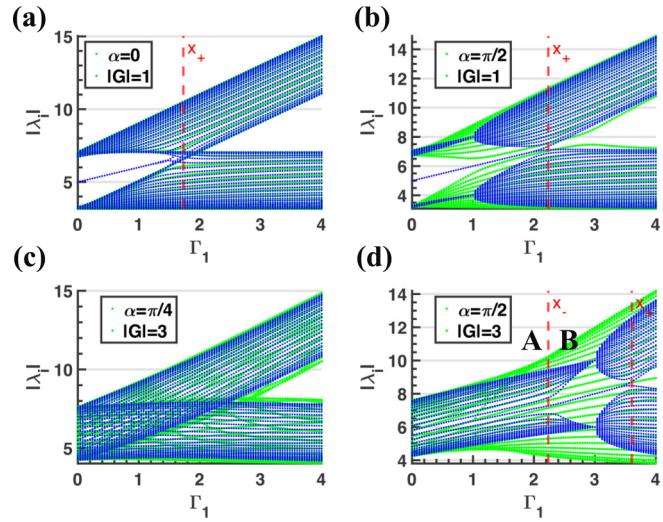

FIG. 5. The absolute value of eigenvalues of H_{full} under OBC (blue) and PBC (green) for different values of α and $|G|$ with $\Gamma_2 = 2$, $\gamma = 3$, the number of units cells $N = 25$. The vertical lines represent the points $x_{\pm}$ obtained from Eq. (34) as $x_{\pm} = \sqrt{A_{\pm}}$ for non-negative values of $A_{\pm}$. The two states with complex energy $-i\Gamma_R = -i(\gamma + \Gamma_1 + \Gamma_2)$ appear in the region $\Gamma_1 < x_-$ and $\Gamma_1 < x_+$ as isolated blue lines in the middle in (a), (b), whereas they appear in the region $x_- < \Gamma_1 < x_+$ in (d).

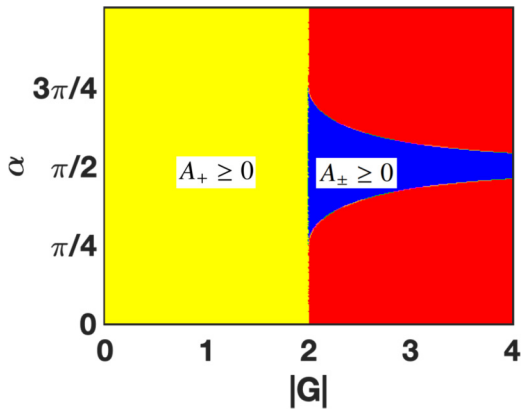

FIG. 6. The phase diagram of the system as a function of α and $|G|$ for $\Gamma_2 = 2$ characterized by the real positive values of $A_\pm$ demarcating the topological boundaries. In particular, the region in red depicts the topologically trivial parametric domain.

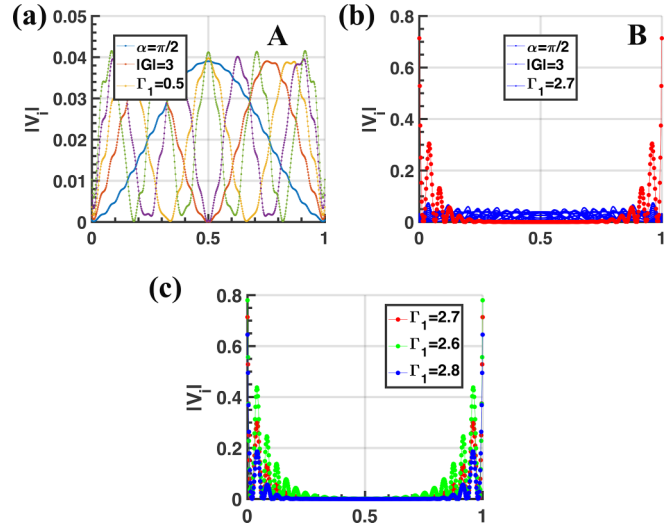

FIG. 7. (a) The absolute value of N components (equally spaced between 0 and 1) of the vector V^i for $i = 1$–5; (b) absolute value of N components of V^i for $i = 1$–N. Note that the red curves in (b) represent the two topological edge-modes of the system (concentrated at both the right and left edges) and we have set the number of unit cells $N = 25$, $\Gamma_2 = 2$, $\gamma = 3$; (c) edge modes of the system for $\Gamma_1 = 2.7$ ($|G| = 3$, $\alpha = \pi/2$) and for two other values of Γ_1 around 2.7 demonstrating the robust nature of localization against any external perturbations. All the N vectors V^i are bulk-modes for $\alpha = \pi/2$, $|G| = 3$ and $\Gamma_1 = 0.5$ and for clarity, we only plot five of them in (a) as the rest of them have similar behavior.

of the system as a function of α and $|G|$ depending on the real positive values of $A_\pm$, clearly demarcating the topological boundaries. For the region depicted in yellow, we have only the $A_+ \geqslant 0$, begetting Γ_R modes for $|\Gamma_1| < \sqrt{A_+}$ as displayed in Figs. 5(a)–5(b). The region in blue, however, provides $A_\pm \geqslant 0$, lending Γ_R modes when $\Gamma_1^2 < A_+$ and $\Gamma_1^2 > A_-$ as demonstrated in Fig. 5(d). In contrast, the region in red prohibits real positive values for $A_\pm$ and therefore does not lend itself to a topological description evident from Fig. 5(c).

To provide more substance to the above discussion, we plot, in Figs. 7(a)–7(b) the absolute value of N components (equally spaced between 0 and 1) of the vector $V^i = [\pi_1^i\ \pi_2^i, \ldots, \pi_N^i\ ]$ for two different regions of Fig. 5(d) with $i \in \{1, 2, \ldots, N\}$ and

$$\pi_n^i = \frac{\langle L_i^{\text{full}} | P_n | R_i^{\text{full}} \rangle}{\langle L_i^{\text{full}} | R_i^{\text{full}} \rangle}, \tag{35}$$

where $|R_i^{\text{full}}\rangle$, $|L_i^{\text{full}}\rangle$ are the right and left eigenvectors of H_{full}, respectively. The Fig. 7(a) corresponds to a point in the topologically trivial region A of Fig. 5(d), that is, for $\alpha = \pi/2$, $\Gamma_1 = 0.5$, $|G| = 3$ hallmarked by the absence of edge modes. In contrast, Fig. 7(b) depicts the absolute value of the projection for $\alpha = \pi/2$, $\Gamma_1 = 2.7$, $|G| = 3$, a point in the region B of Fig. 5(d). Not surprisingly, edge states (in red) springs into existence and they correspond to Eq. (31) matching the two isolated central modes of Fig. 5(d) possessing complex energy $-i\Gamma_R$. To be precise, the two edge modes in Fig. 7 (b) correspond to V^i where $|R_i^{\text{full}}\rangle$, $|L_i^{\text{full}}\rangle$ are replaced, respectively, by the states $|\psi\rangle_R^\pm$ and $|\psi\rangle_L^\pm$. At this point, it is worth noting that any type of disorder in the system would translate into perturbations in the (off-)diagonal elements of the matrix in Eq. (30). For instance, let us consider the topological edge states in Fig. 7(b) for $\Gamma_1 = 2.7$. In Fig. 7(c), we plot the edge states for two different values of Γ_1 around $\Gamma_1 = 2.7$ and $\alpha = \pi/2$, $|G| = 3$. It is apparent from the figure that the population is predominantly localized at the edges of the system testifying to its robustness against external perturbations. On the contrary, the absolute value of the components of eigenvectors $|R_i^{\text{full}}\rangle$ and $|L_i^{\text{full}}\rangle$ would provide starkly dissimilar results with all the eigenstates concentrated at the boundaries, otherwise known as the skin effect. Skin effect, *viz*, the unusual localization of a large number of eigenstates at the boundaries [29,31,32,34,54], a consequence of nonreciprocal coupling, leads to pronounced sensitivity of the bulk to boundary conditions. In Fig. 8(a), we plot $|R_i^{\text{full}}|$, the absolute value of the N components of the column matrix (equally spaced between 0 and 1) representing $|R_i^{\text{full}}\rangle$ for $\alpha = \pi/2$ clearly demonstrating the accumulation of eigenstates at the boundaries of the system owing to the nonreciprocal nature of dissipative coupling. On the contrary, $\alpha = 0$ does not incur any nonreciprocity in coupling, culminating in the absence of skin effect as depicted in Fig. 8(b). In stark contrast to Figs. 8(a), 8(b) the condition $\alpha = \pi/2$ and $|G| = \Gamma_1$ results in $\Gamma_+ \to 0$, i.e., extreme nonreciprocity and skin effect. This is manifested in Fig. 8(c), showcasing the remarkably high localization of the right eigenvectors at the left edge.

VI. CONCLUSIONS

In conclusion, we considered SSH models with a dissipative form of coupling between the subsystems and discussed some of the interesting physics ensuing from such models. In particular, we provided two distinct schemes for the realization of DSSH models in the context of bosonic systems and electrical LCR resonators. We showed that a collection of resistively coupled LCR resonators mimic the topology of DSSH models by solving the Kirchhoff's equation for voltages. In the framework of bosonic systems, we observed that a system of noninteracting oscillators interacting with an engineered bath of modes possessing considerably small

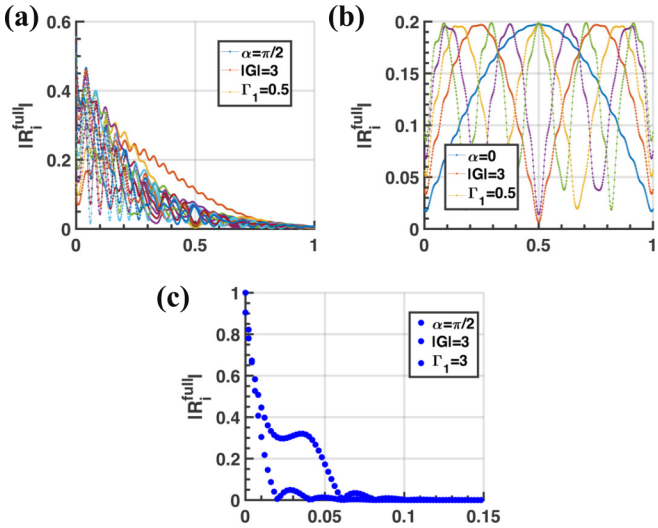

FIG. 8. (a) The absolute value of the eigenvectors (equally spaced between 0 and 1) $|R_i^{\text{full}}\rangle$ for $\alpha = \pi/2$, $|G| = 3$, $\Gamma_1 = 0.5$, clearly demonstrating the eigenmodes, all of which are concentrated on the left edge of the system; (b) absolute value of the eigenvectors $|R_i^{\text{full}}\rangle$ for $\alpha = 0$, $|G| = 3$, $\Gamma_1 = 0.5$ with no nonreciprocity in couplings leading to the absence of edge effects; (c) plot of the absolute value of the eigenvectors $|R_i^{\text{full}}\rangle$ (for the region between zero and 0.15) with $\alpha = \pi/2$, $|G| = 3$, $\Gamma_1 = 3$ with $\Gamma_+ \to 0$ giving rise to extreme nonreciprocity and amplification of edge population when compared to (a). The quantity $|R_i^{\text{full}}|$ is negligibly small beyond 0.15 in (c) and analogous to Fig. 7(a), for clarity, we have only plotted V^i for $i = 1$–5 in (b). The number of unit cells $N = 25$, $\Gamma_2 = 2$, $\gamma = 3$.

lifetimes compared to other system parameters is equivalent to a DSSH model. Further, by enabling the coherent interaction between the oscillators under consideration, we showed that the system affords nonreciprocal dissipative couplings eliciting topological transitions governed by the phase of the coherent interaction strength and skin effect. Note that our analyses are generic, relevant to a large class of systems, especially in microwave to optical settings and merits immediate realization in the experiments.

ACKNOWLEDGMENTS

G.S.A. and M.O.S. acknowledge the support of the Air Force Office of Scientific Research [AFOSR Award No FA9550-20-1-0366] and the Robert A. Welch Foundation (Grants No. A-1261 and No. A-1943-20210327). J.M.P.N. acknowledges the support of the Herman F. Heep and Minnie Belle Heep Texas A&M University endowed fund held/administered by the Texas A&M Foundation.

APPENDIX A: KIRCHHOF'S EQUATIONS FOR THE CIRCUIT DSSH MODEL

We begin by considering the two blocks of LCR circuits, in other words, a dimer, coupled through a resistor as depicted in Fig. 9. After the choice of direction of currents as illustrated in the figure, we use the well-known Kirchoff's circuit laws to explicate the dimer dynamics.

$$I_{R_{c1}} = I_{L_1} + I_{C_1} + I_{R_1} = -(I_{L_2} + I_{C_2} + I_{R_2}), \tag{A1}$$

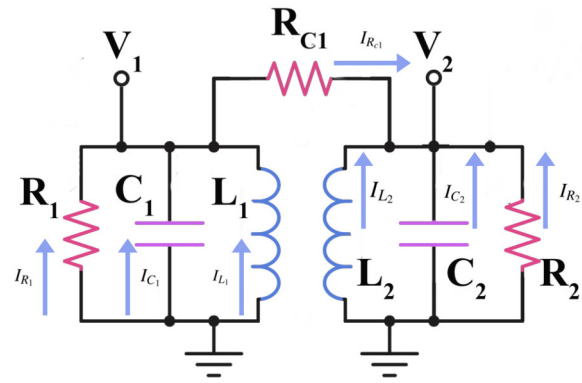

FIG. 9. The unit cell of the circuit SSH model described in Fig. 3. The blue arrows represent the chosen direction currents in the system.

$$V_n = -L_n \frac{dI_{L_n}}{dt} = -\frac{1}{C_n}\int_0^t I_{C_n}(t')dt' = -I_{R_1}R_1, \tag{A2}$$

$$V_1 - V_2 = I_{R_{c1}}R_{c1}, \tag{A3}$$

where $n = 1, 2$. Employing Eq. (A2) and Eq. (A3) into Eq. (A1), we obtain

$$\ddot{V}_i + \frac{1}{C_i}\left(\frac{1}{R_{c1}} + \frac{1}{R_i}\right)\dot{V}_i + \frac{V_i}{L_iC_i} = \frac{\dot{V}_j}{R_{c1}C_i}, \quad i \neq j. \tag{A4}$$

Upon redefining $\omega_i = \frac{1}{\sqrt{L_iC_i}}$, $\Gamma_i = \frac{1}{R_{c1}C_i}$ and $\gamma_i = \frac{1}{R_iC_i}$ Eq. (A4) reduces to

$$\ddot{V}_i + (\gamma_i + \Gamma_i)V_i + \omega_i^2 V_i = \Gamma_i \dot{V}_j, \quad i \neq j. \tag{A5}$$

The Eq. (A5) can be further simplified if we assume $V_i(t) = \frac{1}{2}u_i(t)e^{-i\omega_0 t} + \text{c.c.}$, where $\omega_0 = \frac{1}{2}(\omega_1 + \omega_2)$ and $u_i(t)$ is a slowly varying envelope. In addition, we assume that $k \ll \omega_i$, ω_1 close to ω_2 and $C_1 = C_2$. Under these conditions, the Eq. (A5) can be approximated to

$$\begin{pmatrix}\dot{u}_1\\ \dot{u}_2\end{pmatrix} = -i\frac{1}{2}\begin{pmatrix}\omega_1 - \omega_2 - i(\gamma_1 + \Gamma_1) & i\Gamma_1\\ i\Gamma_1 & \omega_2 - \omega_1 - i(\gamma_2 + \Gamma_1)\end{pmatrix} \times \begin{pmatrix}u_1\\ u_2\end{pmatrix}. \tag{A6}$$

Extending the analysis to the full system in Fig. 3, we obtain Eq. (15).

APPENDIX B: WEAK COUPLING DOMAIN FOR THE DSSH MODEL

Consider the dynamics of the mode a_1 from Eq. (20) in the frame rotating at frequency $\omega_{a,1}$ provided by

$$\dot{a}_1 = -\kappa_1 a_1 - ig(b_1 - c_1). \tag{B1}$$

Formally integrating the above equation renders

$$a_1(t) = a_1(0)e^{-\kappa_1 t} - i\int_0^t g[b_1(t') - c_1(t')]e^{-\kappa_1(t-t')}. \tag{B2}$$

Note, however, we are interested in the dynamics of the system at t such that $\frac{1}{\kappa_1} \ll t \ll \frac{1}{\gamma}, \frac{1}{g}$. Therefore, the first term

on the RHS of the above equation fades in importance. Additionally, b_1 and c_1 possessing larger decay times can be taken out of the integral from the second term on the RHS of Eq. (B2) culminating in $a_1(t) = -ig\frac{(b_1-c_1)}{\kappa_1}$. Subsequently, we can use this expression to adiabatically eliminate a_1 from the dynamical equation of motions for b_1 and c_1. By the same token, one can also eliminate the mode d_1 to obtain an effective interaction between b_1 and c_1. Upon extending the analysis into the full system given in Eq. (20) and moving into the Fourier domain, we obtain Eq. (21).

[1] M. Z. Hasan and C. L. Kane, Colloquium: Topological insulators, Rev. Mod. Phys. **82**, 3045 (2010).

[2] X.-L. Qi and S.-C. Zhang, Topological insulators and superconductors, Rev. Mod. Phys. **83**, 1057 (2011).

[3] T. Ozawa, H. M. Price, A. Amo, N. Goldman, M. Hafezi, L. Lu, M. C. Rechtsman, D. Schuster, J. Simon, O. Zilberberg, and I. Carusotto, Topological photonics, Rev. Mod. Phys. **91**, 015006 (2019).

[4] L. Lu, J. D. Joannopoulos, and M. Soljačić, Topological photonics, Nature Photonics **8**, 821 (2014).

[5] J. Dalibard, F. Gerbier, G. Juzeliūnas, and P. Öhberg, Colloquium: Artificial gauge potentials for neutral atoms, Rev. Mod. Phys. **83**, 1523 (2011).

[6] R. Süsstrunk and S. D. Huber, Observation of phononic helical edge states in a mechanical topological insulator, Science **349**, 47 (2015).

[7] C. Kane and T. Lubensky, Topological boundary modes in isostatic lattices, Nature Phys. **10**, 39 (2014).

[8] J. Paulose, B. G.-g. Chen, and V. Vitelli, Topological modes bound to dislocations in mechanical metamaterials, Nature Phys. **11**, 153 (2015).

[9] A. Y. Kitaev, Unpaired majorana fermions in quantum wires, Phys. Usp. **44**, 131 (2001).

[10] J. Q. You, X.-F. Shi, X. Hu, and F. Nori, Quantum emulation of a spin system with topologically protected ground states using superconducting quantum circuits, Phys. Rev. B **81**, 014505 (2010).

[11] J. Alicea, Y. Oreg, G. Refael, F. Von Oppen, and M. Fisher, Non-abelian statistics and topological quantum information processing in 1d wire networks, Nature Phys. **7**, 412 (2011).

[12] X.-J. Liu, Z.-X. Liu, and M. Cheng, Manipulating topological edge spins in a one-dimensional optical lattice, Phys. Rev. Lett. **110**, 076401 (2013).

[13] J. Q. You, Z. D. Wang, W. Zhang, and F. Nori, Encoding a qubit with Majorana modes in superconducting circuits, Sci. Rep. **4**, 5535 (2014).

[14] P. St-Jean, V. Goblot, E. Galopin, A. Lemaître, T. Ozawa, L. Le Gratiet, I. Sagnes, J. Bloch, and A. Amo, Lasing in topological edge states of a one-dimensional lattice, Nature Photon. **11**, 651 (2017).

[15] B. Bahari, A. Ndao, F. Vallini, A. El Amili, Y. Fainman, and B. Kanté, Nonreciprocal lasing in topological cavities of arbitrary geometries, Science **358**, 636 (2017).

[16] G. Harari, M. A. Bandres, Y. Lumer, M. C. Rechtsman, Y. D. Chong, M. Khajavikhan, D. N. Christodoulides, and M. Segev, Topological insulator laser: Theory, Science **359**, eaar4003 (2018).

[17] M. A. Bandres, S. Wittek, G. Harari, M. Parto, J. Ren, M. Segev, D. N. Christodoulides, and M. Khajavikhan, Topological insulator laser: Experiments, Science **359**, eaar4005 (2018).

[18] J. Perczel, J. Borregaard, D. E. Chang, H. Pichler, S. F. Yelin, P. Zoller, and M. D. Lukin, Topological quantum optics in two-dimensional atomic arrays, Phys. Rev. Lett. **119**, 023603 (2017).

[19] J.-S. Pan, X.-J. Liu, W. Zhang, W. Yi, and G.-C. Guo, Topological superradiant states in a degenerate Fermi gas, Phys. Rev. Lett. **115**, 045303 (2015).

[20] F. Mivehvar, H. Ritsch, and F. Piazza, Superradiant topological peierls insulator inside an optical cavity, Phys. Rev. Lett. **118**, 073602 (2017).

[21] P. Doyeux, S. A. H. Gangaraj, G. W. Hanson, and M. Antezza, Giant interatomic energy-transport amplification with nonreciprocal photonic topological insulators, Phys. Rev. Lett. **119**, 173901 (2017).

[22] W. Nie, Z. H. Peng, F. Nori, and Y. X. Liu, Topologically protected quantum coherence in a superatom, Phys. Rev. Lett. **124**, 023603 (2020).

[23] W. Nie, M. Antezza, Y. X. Liu, and F. Nori, Dissipative topological phase transition with strong system-environment coupling, Phys. Rev. Lett. **127**, 250402 (2021).

[24] S. Barik, A. Karasahin, C. Flower, T. Cai, H. Miyake, W. DeGottardi, M. Hafezi, and E. Waks, A topological quantum optics interface, Science **359**, 666 (2018).

[25] J. Jiang, J. Ren, Z. Guo, W. Zhu, Y. Long, H. Jiang, and H. Chen, Seeing topological winding number and band inversion in photonic dimer chain of split-ring resonators, Phys. Rev. B **101**, 165427 (2020).

[26] G. S. Agarwal, *Quantum Statistical Theories of Spontaneous Emission and Their Relation to Other Approaches*, edited by G. Hhler Quantum Optics. Springer Tracts in Modern Physics, Vol 70 (Springer, Berlin, Heidelberg, 1974).

[27] E. J. Bergholtz, J. C. Budich, and F. K. Kunst, Exceptional topology of non-Hermitian systems, Rev. Mod. Phys. **93**, 015005 (2021).

[28] Z. Gong, Y. Ashida, K. Kawabata, K. Takasan, S. Higashikawa, and M. Ueda, Topological phases of non-Hermitian systems, Phys. Rev. X **8**, 031079 (2018).

[29] T. E. Lee, Anomalous edge state in a non-Hermitian lattice, Phys. Rev. Lett. **116**, 133903 (2016).

[30] Y. Xiong, Why does bulk boundary correspondence fail in some non-Hermitian topological models, J. Phys. Commun. **2**, 035043 (2018).

[31] S. Yao and Z. Wang, Edge states and topological invariants of non-Hermitian systems, Phys. Rev. Lett. **121**, 086803 (2018).

[32] F. K. Kunst, E. Edvardsson, J. C. Budich, and E. J. Bergholtz, Biorthogonal bulk-boundary correspondence in non-Hermitian systems, Phys. Rev. Lett. **121**, 026808 (2018).

[33] F. K. Kunst and V. Dwivedi, Non-Hermitian systems and topology: A transfer-matrix perspective, Phys. Rev. B **99**, 245116 (2019).

[34] C. H. Lee and R. Thomale, Anatomy of skin modes and topology in non-Hermitian systems, Phys. Rev. B **99**, 201103(R) (2019).

[35] K. Kawabata, M. Sato, and K. Shiozaki, Higher-order non-Hermitian skin effect, Phys. Rev. B **102**, 205118 (2020).
[36] L. Xiao, T. Deng, K. Wang, G. Zhu, Z. Wang, W. Yi, and P. Xue, Non-Hermitian bulk–boundary correspondence in quantum dynamics, Nature Phys. **16**, 761 (2020).
[37] S. Guo, C. Dong, F. Zhang, J. Hu, and Z. Yang, Theoretical prediction of a non-Hermitian skin effect in ultracold-atom systems, Phys. Rev. A **106**, L061302 (2022).
[38] V. M. Martinez Alvarez, J. E. Barrios Vargas, and L. E. F. Foa Torres, Non-Hermitian robust edge states in one dimension: Anomalous localization and eigenspace condensation at exceptional points, Phys. Rev. B **97**, 121401(R) (2018).
[39] K. Deng and B. Flebus, Non-Hermitian skin effect in magnetic systems, Phys. Rev. B **105**, L180406 (2022).
[40] N. Malkova, I. Hromada, X. Wang, G. Bryant, and Z. Chen, Observation of optical shockley-like surface states in photonic superlattices, Opt. Lett. **34**, 1633 (2009).
[41] W. Tan, Y. Sun, H. Chen, and S.-Q. Shen, Photonic simulation of topological excitations in metamaterials, Sci. Rep. **4**, 1 (2014).
[42] J. M. Zeuner, M. C. Rechtsman, Y. Plotnik, Y. Lumer, S. Nolte, M. S. Rudner, M. Segev, and A. Szameit, Observation of a topological transition in the bulk of a non-Hermitian system, Phys. Rev. Lett. **115**, 040402 (2015).
[43] F. Bleckmann, Z. Cherpakova, S. Linden, and A. Alberti, Spectral imaging of topological edge states in plasmonic waveguide arrays, Phys. Rev. B **96**, 045417 (2017).
[44] C. H. Lee, S. Imhof, C. Berger, F. Bayer, J. Brehm, L. W. Molenkamp, T. Kiessling, and R. Thomale, Topolectrical circuits, Commun. Phys. **1**, 39 (2018).
[45] C. Yin, H. Jiang, L. Li, R. Lü, and S. Chen, Geometrical meaning of winding number and its characterization of topological phases in one-dimensional chiral non-Hermitian systems, Phys. Rev. A **97**, 052115 (2018).
[46] X. Zhao, Y. Xing, L. Qi, S. Liu, S. Zhang, and H.-F. Wang, Real-potential-driven anti–symmetry breaking in non-Hermitian Su–Schrieffer–Heeger model, New J. Phys. **23**, 073043 (2021).
[47] S. Lieu, Topological phases in the non-Hermitian Su-Schrieffer-Heeger model, Phys. Rev. B **97**, 045106 (2018).
[48] S. Tsubota, H. Yang, Y. Akagi, and H. Katsura, Symmetry-protected quantization of complex berry phases in non-Hermitian many-body systems, Phys. Rev. B **105**, L201113 (2022).
[49] L. Qi, G.-L. Wang, S. Liu, S. Zhang, and H.-F. Wang, Engineering the topological state transfer and topological beam splitter in an even-sized Su-Schrieffer-Heeger chain, Phys. Rev. A **102**, 022404 (2020).
[50] H. Schomerus, Topologically protected midgap states in complex photonic lattices, Opt. Lett. **38**, 1912 (2013).
[51] C. C. Wanjura, M. Brunelli, and A. Nunnenkamp, Topological framework for directional amplification in driven-dissipative cavity arrays, Nature Commun. **11**, 3149 (2020).
[52] M. Brunelli, C. C. Wanjura, and A. Nunnenkamp, Restoration of the non-Hermitian bulk-boundary correspondence via topological amplification, SciPost Phys. **15**, 173 (2023).
[53] D. Porras and S. Fernández-Lorenzo, Topological amplification in photonic lattices, Phys. Rev. Lett. **122**, 143901 (2019).
[54] V. M. Vyas and D. Roy, Topological aspects of periodically driven non-Hermitian Su-Schrieffer-Heeger model, Phys. Rev. B **103**, 075441 (2021).
[55] D. Halder, S. Ganguly, and S. Basu, Properties of the non-Hermitian SSH model: Role of symmetry, J. Phys.: Condens. Matter **35**, 105901 (2023).
[56] C. Leefmans, A. Dutt, J. Williams, L. Yuan, M. Parto, F. Nori, S. Fan, and A. Marandi, Topological dissipation in a time-multiplexed photonic resonator network, Nature Phys. **18**, 442 (2022).
[57] D. Hao, L. Wang, X. Lu, X. Cao, S. Jia, Y. Hu, and Y. Xiao, Topological atomic spin wave lattices by dissipative couplings, Phys. Rev. Lett. **130**, 153602 (2023).
[58] G. S. Agarwal, *Quantum Optics* (Cambridge University Press, Cambridge, 2012).
[59] A. Metelmann and A. A. Clerk, Nonreciprocal photon transmission and amplification via reservoir engineering, Phys. Rev. X **5**, 021025 (2015).
[60] G. S. Agarwal and R. R. Puri, Cooperative behavior of atoms irradiated by broadband squeezed light, Phys. Rev. A **41**, 3782 (1990).
[61] A. McDonald, R. Hanai, and A. A. Clerk, Nonequilibrium stationary states of quantum non-Hermitian lattice models, Phys. Rev. B **105**, 064302 (2022).
[62] Y. Choi, C. Hahn, J. W. Yoon, and S. H. Song, Observation of an anti-PT-symmetric exceptional point and energy-difference conserving dynamics in electrical circuit resonators, Nature Commun. **9**, 2182 (2018).
[63] D. Mukhopadhyay and G. S. Agarwal, Multiple fano interferences due to waveguide-mediated phase coupling between atoms, Phys. Rev. A **100**, 013812 (2019).
[64] D. Mukhopadhyay and G. S. Agarwal, Transparency in a chain of disparate quantum emitters strongly coupled to a waveguide, Phys. Rev. A **101**, 063814 (2020).
[65] H. Zhang, R. Huang, S.-D. Zhang, Y. Li, C.-W. Qiu, F. Nori, and H. Jing, Breaking anti-PT symmetry by spinning a resonator, Nano Lett. **20**, 7594 (2020).
[66] J. M. Silver, L. Del Bino, M. T. Woodley, G. N. Ghalanos, A. Ø. Svela, N. Moroney, S. Zhang, K. T. Grattan, and P. Del'Haye, Nonlinear enhanced microresonator gyroscope, Optica **8**, 1219 (2021).
[67] M. Harder, Y. Yang, B. M. Yao, C. H. Yu, J. W. Rao, Y. S. Gui, R. L. Stamps, and C.-M. Hu, Level attraction due to dissipative magnon-photon coupling, Phys. Rev. Lett. **121**, 137203 (2018).
[68] P.-C. Xu, J. W. Rao, Y. S. Gui, X. Jin, and C.-M. Hu, Cavity-mediated dissipative coupling of distant magnetic moments: Theory and experiment, Phys. Rev. B **100**, 094415 (2019).
[69] Y.-P. Wang, J. W. Rao, Y. Yang, P.-C. Xu, Y. S. Gui, B. M. Yao, J. Q. You, and C.-M. Hu, Nonreciprocity and unidirectional invisibility in cavity magnonics, Phys. Rev. Lett. **123**, 127202 (2019).
[70] J. M. P. Nair, D. Mukhopadhyay, and G. S. Agarwal, Enhanced sensing of weak anharmonicities through coherences in dissipatively coupled anti-PT symmetric systems, Phys. Rev. Lett. **126**, 180401 (2021).
[71] J. M. P. Nair, D. Mukhopadhyay, and G. S. Agarwal, Ultralow threshold bistability and generation of long-lived mode in a dissipatively coupled nonlinear system: Application to magnonics, Phys. Rev. B **103**, 224401 (2021).
[72] F. K. Kunst, G. van Miert, and E. J. Bergholtz, Lattice models with exactly solvable topological Hinge and Corner states, Phys. Rev. B **97**, 241405(R) (2018).